Natural convection between two concentric spheres: transition toward a multicellular flow

Jean-Paul Caltagirone, M. Combarnous, Abdelkader Mojtabi

NATURAL CONVECTION BETWEEN TWO CONCENTRIC SPHERES: TRANSITION TOWARD A MULTICELLULAR FLOW

J.-P. Caltagirone
Laboratoire d'Aérothermique du C.N.R.S.,
F 92190 Meudon, France

M. Combarnous
Laboratoire de Mécanique Physique, ERA-C.N.R.S. 769
Université de Bordeaux I, France

A. Mojtabi
Laboratoire d'Aérothermique du C.N.R.S.,
F 92190 Meudon, France

A moderate temperature difference maintained between two concentric spherical surfaces induces, in steady state, unicellular toroidal movements in the enclosed fluid. Beyond a critical temperature difference, the flow becomes unstable and the convective phenomena rearrange into counter-rotating toroidal cells. A two-dimensional axisymmetric numerical model confirms the existence of a unicellular regime and shows that, beyond the critical conditions and for the same set of parameters, two convergent solutions can be obtained. One is unicellular and the other is bicellular; in the latter, the additional cell appears at the top of the layer. The initial conditions determine which one of these two will be established. This transition is investigated as a function of several parameters and the results are compared with the experimental results in the literature.

INTRODUCTION

The flow due to natural convection between two concentric spheres has been widely investigated experimentally. The different types of flow and the global heat transfer were sought.

For radius ratios between 1.19 and 3.14 and air, Bishop et al. [1] distinguished three types of flow. Most frequently, a two-dimensional, crescent-shaped, unicellular flow was encountered. For a radius ratio of 1.37 or 1.72, this was the only type of flow obtained, regardless of the temperature difference between the two spheres. For moderate or high temperature gradients and radius ratios of 2.53 and 3.14, a kidney-shaped cell was observed.

A third type of flow was observed for small radius ratios (1.19) and moderate or high temperature differences. This flow is unsteady and multicellular. Small cells appear and disappear periodically at the top of the layer. The measured temperature profiles agree with the types of flow mentioned.

Scanlan et al. [2] used water and two silicone oils to investigate this flow. The Prandtl number varied from 4.7 to 4148 and radius ratios between 1.09 and 2.8 were

NOMENCLATURE

r_i, r_o	inner and outer sphere radii	ϕ	azimuthal angle
R	ratio of outer to inner sphere radius ($= r_o/r_i$)	λ	thermal conductivity
		ν	kinematic viscosity
Ra	Rayleigh number [$= g\alpha\rho c(T_i - T_o)r_i^3/\lambda\nu$]	ρ_1	reference density
		θ	angular coordinate measured from downward polar axis
Ra_L	Rayleigh number based on layer thickness [$= (R-1)^3\,\mathrm{Ra}$]	Ψ	stream function
Pr	Prandtl number ($= \nu\rho c/\lambda$)	ω	vorticity
T	temperature [$= (T' - T_o)/(T_i - T_o)$]		
T_i, T_o	inner and outer sphere temperatures	**Superscript**	
T_1'	reference temperature		
α	coefficient of thermal expansion		real variable

considered. The global Nusselt number is plotted as a function of the Rayleigh number for all three liquids.

Yin et al. [3], for water and air and radius ratios between 1.09 and 2.17, obtain two experimental curves; for each fluid, the transition Grashof number, transition between the steady and unsteady flows, is given as a function of the ratio of the inner sphere diameter to the annular thickness.

Mack and Hardee [4] determined, by the perturbation method developed up to order 3, the temperature and stream function fields. This method is valid only for small Rayleigh numbers; thus, no conclusions on the convergence as a function of the Rayleigh number are possible.

Here, a numerical model using the implicit alternating direction method permits the temperature and stream function field to be obtained. Radius ratios between 1.15 and 3 and Rayleigh numbers varying from 100 to 10^5 are considered. For a given set of parameters, two different solutions are possible.

THEORETICAL FORMULATION

A fluid layer lies between two concentric spheres. The inner sphere, of radius r_i, is kept at a constant temperature T_i, while the outer sphere, of radius r_o, is kept at a constant but lower temperature T_o ($T_i > T_o$). The properties of the fluid layer are: a coefficient of thermal expansion α, a kinematic viscosity ν, a specific heat per unit volume ρc, and a thermal conductivity λ, all defined at a reference temperature T_1'.

The governing equations are:

$$\nabla \cdot \mathbf{V}' = 0 \tag{1}$$

$$\frac{\partial T'}{\partial t'} - \frac{\lambda}{\rho c}\nabla^2 T' + \mathbf{V}' \cdot \nabla T' = 0 \tag{2}$$

$$\rho\left(\frac{\partial \mathbf{V}'}{\partial t'} + \mathbf{V}' \cdot \nabla \mathbf{V}'\right) + \nabla P - \rho \mathbf{g} - \rho\nu\nabla^2 \mathbf{V}' = 0 \tag{3}$$

$\mathbf{V}' = V_r'\mathbf{e}_1 + V_\theta'\mathbf{e}_2 + V_\phi'\mathbf{e}_3$ is the fluid velocity; T' is the temperature; P' is the pressure; $\mathbf{g} = -g\mathbf{k}$ is the acceleration due to gravity; $\mathbf{e}_1, \mathbf{e}_2, \mathbf{e}_3$ are unit normal vectors; and $\mathbf{k} = \cos\theta\,\mathbf{e}_1 - \sin\theta\,\mathbf{e}_2$.

The fluid state equation is:

$$\rho = \rho_1 [1 - \alpha(T' - T_1')]$$

The Boussinesq approximation is assumed valid. To render the equations dimensionless, the reference values r_i, $\rho c r_i^2/\lambda$, $\lambda/r_i \rho c$, $r_i^2 \rho c^2/\lambda^2$, and $\Delta T' = T_i - T_o$ are used for length, time, pressure, and temperature, respectively. Since the flow is axisymmetric, only half the enclosed region is considered.

For this two-dimensional domain, and introducing the stream function Ψ, the dimensionless equations are:.

$$D^2 \Psi = -\omega \tag{4}$$

$$\frac{\partial T}{\partial t} = \nabla^2 T - \frac{1}{r^2 \sin\theta}\left(\frac{\partial \Psi}{\partial \theta}\frac{\partial T}{\partial r} - \frac{\partial \Psi}{\partial r}\frac{\partial T}{\partial \theta}\right) \tag{5}$$

$$\frac{\partial \omega}{\partial t} = -\mathrm{Pr}\ \mathrm{Ra}\, r \sin\theta \left(\sin\theta \frac{\partial T}{\partial r} + \frac{\cos\theta}{r}\frac{\partial T}{\partial \theta}\right) + \mathrm{Pr}\, D^2 \omega$$
$$- \sin\theta \left(\frac{\partial \Psi}{\partial \theta}\frac{\partial}{\partial r} - \frac{\partial \Psi}{\partial r}\frac{\partial}{\partial \theta}\right)\left(\frac{\omega}{r^2 \sin^2\theta}\right) \tag{6}$$

$$V_r = \frac{1}{r^2 \sin\theta}\frac{\partial \Psi}{\partial \theta} \qquad V_\phi = \frac{-1}{r \sin\theta}\frac{\partial \Psi}{\partial r}$$

$$\nabla^2 = \frac{\partial^2}{\partial r^2} + \frac{2}{r}\frac{\partial}{\partial r} + \frac{1}{r^2 \tan\theta}\frac{\partial}{\partial \theta} + \frac{1}{r^2}\frac{\partial^2}{\partial \theta^2}$$

$$D^2 = \frac{\partial^2}{\partial r^2} + \frac{1}{r^2}\frac{\partial^2}{\partial \theta^2} - \frac{1}{r^2}\cot\theta \frac{\partial}{\partial \theta}$$

θ starts from the descending vertical.

Apart from $R = r_o/r_i$, which describes the system's geometry, two dimensionless parameters appear in the equations, the Rayleigh number $\mathrm{Ra} = g\alpha\rho c\, \Delta T' r_i^3/\lambda\nu$ and the Prandtl number $\mathrm{Pr} = \nu\rho c/\lambda$. Another Rayleigh number, based on the layer thickness $L = r_o - r_i$, will be used later and is $\mathrm{Ra}_L = \mathrm{Ra}\,(R-1)^3$.

The boundary conditions are:

$$\Psi = \frac{\partial \Psi}{\partial r} = 0 \qquad T = 1 \qquad \text{for } r = 1 \tag{7}$$

$$\Psi = \frac{\partial \Psi}{\partial r} = 0 \qquad T = 0 \qquad \text{for } R = r = \frac{r_o}{r_i} \tag{8}$$

$$\Psi = 0 \qquad \frac{\partial T}{\partial \theta} = 0 \qquad \text{for } \theta = 0 \text{ and } \pi \tag{9}$$

There are no boundary conditions for the vorticity, but indirectly

$$\omega = -\frac{\partial^2 \Psi}{\partial r^2} \qquad \text{for } r = 1 \text{ and } R$$
$$\omega = 0 \qquad \text{for } \theta = 0 \text{ and } \pi \tag{10}$$

The local heat transfer is determined by the local Nusselt number:

$$\mathrm{Nu} = \left(V_r T - \frac{\partial T}{\partial r}\right) r \log R$$

Hotter Outer Sphere Case

Let the subscripts 1 and 2 denote the flow solutions when the inner sphere is kept at a higher temperature and a lower temperature, respectively. Direct substitution into Eqs. (4)-(6) leads immediately to:

$$\begin{aligned} \Psi_2(r, \theta) &= -\Psi_1(r, \pi - \theta) \\ \omega_2(r, \theta) &= -\omega_1(r, \pi - \theta) \\ T_2(r, \theta) &= 1 - T_1(r, \pi - \theta) \end{aligned} \tag{11}$$

NUMERICAL MODEL

Equation (4) is modified in order to introduce a fictitious time ρ:

$$\frac{\partial \Psi}{\partial \rho} = D^2 \Psi + \omega \tag{4a}$$

Keeping the time-dependent terms allows the introduction of the initial conditions naturally and the acquisition of the steady solution without necessarily being concerned with nonstationary behavior.

The system of Eqs. (4*a*)-(9) is formulated in finite differences and solved by the implicit alternating direction scheme. A calculation for a given Ra_L, Pr, and R is developed as follows. Initial temperature and stream function fields are introduced. The vorticity boundary conditions are calculated using the unsteady form of Eq. (10):

$$\frac{\partial \omega}{\partial t} + \omega + \frac{\partial^2 \Psi}{\partial r^2} = 0 \tag{10a}$$

Equation (6) is used to obtain the vorticity field and Eq. (4*a*) the stream function; then Eq. (5) is solved to obtain the temperature fields, and finally the total Nusselt number is calculated within the same time step. A cycle corresponding to a new time step is then started. Calculations continue until the solution converges over the whole range. Tests based on the global Nusselt number then stop the calculation. At every time step the local Nusselt number and the global Nusselt number are printed. The time for calculation with a 49×49 network for $1 < r < R$ and $0 < \theta < \pi$ is 7 s per time step on an IBM 370-168 computer.

The initial temperature distribution is either pure conduction or a particular distribution inducing downward velocity in the upper part of the layer. The first of these last initial conditions is:

$$T_o(r, \theta) = 1 - \frac{\ln r}{\ln R} + \alpha \sin\left(\pi \frac{\log r}{\log R}\right) \cos \gamma\theta \tag{12}$$

α is an amplitude coefficient and γ is a wave number that makes it possible to introduce either a symmetrical or a nonsymmetrical temperature field with respect to the vertical axis. When Ra is very important, the nonsymmetrical temperature field leads to a downward velocity along the vertical axis in the upper part of the layer; but for moderate Rayleigh numbers, it is not possible to have a downward velocity in the upper part of the layer with an initial temperature field such as Eq. (12). We then abandon Eq. (12) and choose the same initial condition for all our calculations every time there is a relatively important downward velocity in the upper part of the layer. This last initial condition corresponds to a numerical initial temperature and velocity fields with a counter-rotating cell at the top of the layer. For small Rayleigh numbers, this initial condition with a counter-rotating cell leads to unicellular flow, just like the initial condition corresponding to pure conduction.

Depending on the Rayleigh number, steady profiles are obtained after 50-80 iterations. Isotherms and streamlines are plotted at the end of each calculation.

RESULTS AND DISCUSSION

The results are discussed and reference is made to two recent publications; the first, by Charrier-Mojtabi et al. [5], treats natural convection between two cylinders, and the second, by Fauveau et al. [6], considers a porous layer between two spheres.

Figure 1 shows, for $Pr = 0.7$, the Nusselt number plotted against the Rayleigh number for a radius ratio of 2. The numerical values of the parameters and the most significant results obtained are given in Table 1. For a given radius ratio and a relatively high Rayleigh number, Fig. 1 shows two different numerical values for the steady-state Nusselt number.

Each curve in Fig. 1 was calculated in the following way: points on curve (*a*) were computed from the initial conditions corresponding to pure conduction. For curve (*b*), all the points were obtained starting from the same initial condition corresponding to relatively important downward velocity along the vertical axis, in the upper part of the layer.

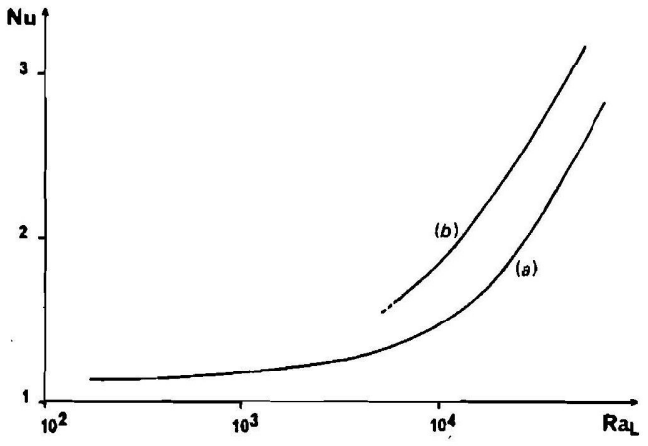

Fig. 1 Nusselt number as a function of Rayleigh number for $R = 2$.

Table 1 Values of Nu, Ψ_{max}, and $V_r[\theta = \pi, r = (R + 1)/2]$ Calculated as Functions of Ra_L and R

R	Ra_L	Nu	Ψ_{max}	V_r
1.2	6,000	1.24	14.81	23.20
	6,000	1.28	15.3	−87
$\sqrt{2}$	3,000	1.11	5.11	12.43
	3,000	1.26	6.51	−14.48
	5,000	1.40	9.18	−18.43
2	10,000	1.18	4.0	9
	5,000	1.30	5.48	14.55
	5,000	1.60	10.2	−2
	10,000	1.47	7.38	17.97
	10,000	1.89	13.33	−14.02
	30,000	2.65	23.57	−63.20
	50,000	2.58	19.30	41.52
	50,000	3.12	29.28	−76.61

These two cases correspond to two different flows: case (a) is unicellular toroidal and case (b) is multicellular toroidal. In the latter, the temperature and stream function fields are almost identical to those of case (a) for $0 < \theta < 120°$. However, at the top, a counter-rotating cell of smaller magnitude appears. Figures 2 and 3 shows the temperature and streamlines obtained for case (a) and case (b) for two different radius ratios ($R = \sqrt{2}$ and 2).

The multicellular regime, which is both experimentally and numerically confirmed for a spherical porous medium [7], suggests some comparison despite the obvious differences [8] between the Darcy and Navier-Stokes equations. In both porous and fluid media the unicellular regime is easier to obtain numerically, and in both the multicellular regime is obtained if a negative velocity is imposed, at the top,

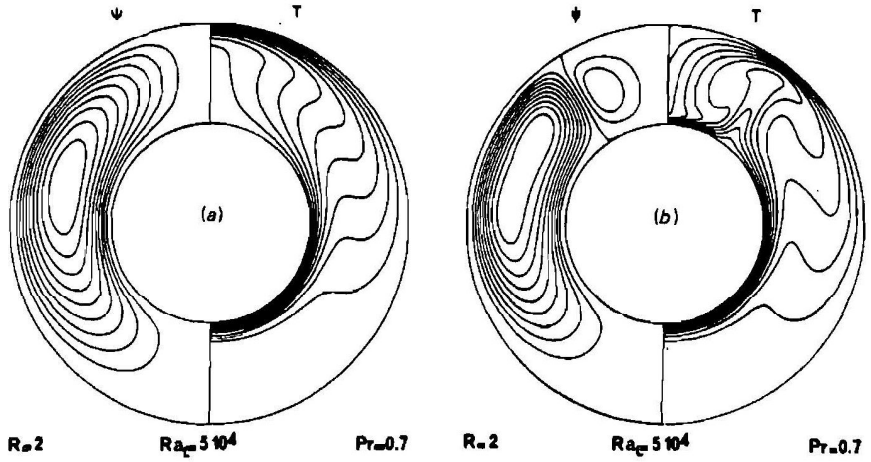

Fig. 2 Streamlines and isotherms for $R = \sqrt{2}$, $Pr = 0.7$, and $Ra_L = 3000$.

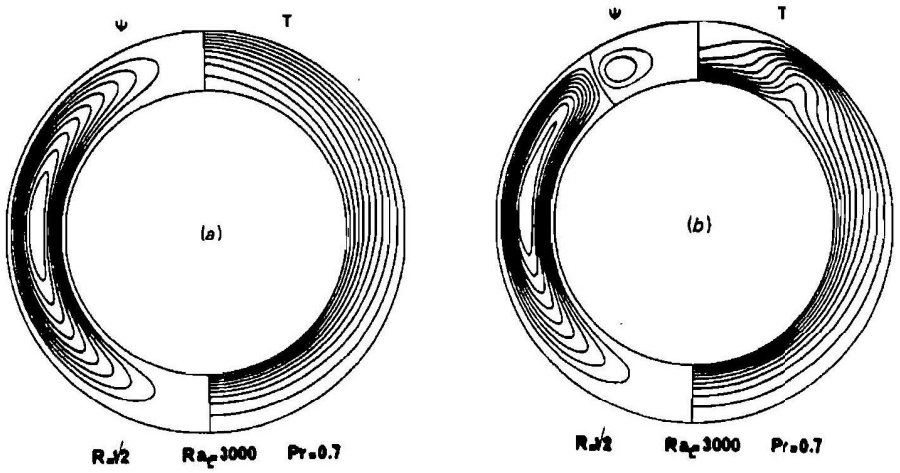

Fig. 3 Streamlines and isotherms for $R = 2$, Pr = 0.7, and $Ra_L = 50{,}000$.

by the initial conditions. This work is limited to $Ra_L = 5 \times 10^4$ for $R = 2$. If the value were much higher, the multicellular regime could appear spontaneously. If this were so, a critical Rayleigh number, beyond which the unicellular regime is no longer possible, would thus be defined.

The multicellular regime observed by Bishop et al. [1] is unsteady but nothing proves that it cannot be axisymmetric, multicellular regime does exist; however, the Nusselt number values oscillate before the solution converges to the steady state. For the unicellular case, the oscillations are barely noticeable and convergence is much faster.

Two things could explain the incongruence between the numerical calculations and the experimental data: either a two-dimensional model is insufficient to show the unsteady behavior, or the time step size corresponds to a real time that is greater than the period of oscillation (9-12 s); the calculations combine phenomena with different characteristic times.

The multicellular regime is very different from the one obtained for a horizontal cylindrical layer. Charrier-Mojtabi et al. [5] used analogous initial conditions and, for high Rayleigh numbers ($Ra_L = 50 \times 10^3$), were unable to obtain a multicellular regime for Pr = 0.7.

The numerical, axisymmetric model used here is a logical but not the final step in the understanding of the convective phenomena between two spheres. A three-dimensional analysis would be necessary to determine whether the counter-rotating cells are axisymmetric or three-dimensional.

To emphasize the difference between these two solutions, the radial velocity, at $\theta = \pi$ and $r = (R + 1)/2$, is plotted in Fig. 4 as a function of the Rayleigh number for $R = 2$. A critical Rayleigh number, beyond which the two solutions can coexist, can be approximately defined. Below this critical Rayleigh number Ra_c, only the unicellular regime is possible.

CONCLUDING REMARKS

At the state of development of this study, two points can be emphasized as general concluding remarks concerning an axisymmetric two-dimensional model in this configuration:

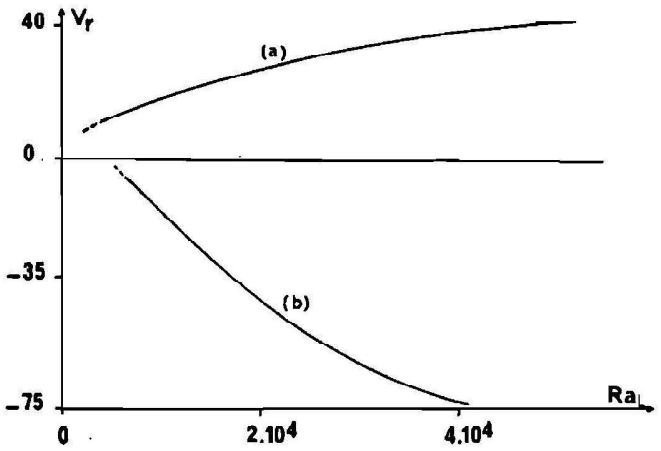

Fig. 4 Radial velocity at $\theta = \pi$ and $r = (R + 1)/2$ as a function of Rayleigh number for $R = 2$.

1. Because several numerical solutions can be obtained, the physical solution must be revealed by complementary experimental or three-dimensional studies.
2. In numerical work, unicellular flow tends to appear much more readily than the multicellular regime. This observation, which can often be considered for high Rayleigh numbers as contradicting reality, is probably a consequence of the assumption of axisymmetric flow, which therefore appears too restrictive.

REFERENCES

1. E. H. Bishop, L. R. Mack, and J. A. Scanlan, Heat Transfer by Natural Convection Between Concentric Spheres, *Int. J. Heat Mass Transfer*, vol. 9, pp. 649–661, 1966.
2. J. A. Scanlan, E. H. Bishop, and R. E. Powe, Natural Convection Heat Transfer Between Concentric Spheres, *Int. J. Heat Mass Transfer*, vol. 13, pp. 1857–1871.
3. S. H. Yin, R. E. Powe, J. A. Scanlan, and E. H. Bishop, Natural Convection Flow Patterns in Spherical Annuli, *Int. J. Heat Mass Transfer*, vol. 16, pp. 1785–1795, 1973.
4. L. R. Mack and H. C. Hardee, Natural Convection Between Concentric Spheres at Low Rayleigh Numbers, *Int. J. Heat Mass Transfer*, vol. 11, pp. 387–396, 1968.
5. M. C. Charrier-Mojtabi, A. Mojtabi, and J.-P. Caltagirone, Numerical Solution of a Flow Due to Natural Convection in a Horizontal Cylindrical Annulus, *J. Heat Transfer, Trans. ASME*, ser. C, vol. 101, pp. 171–173, 1979.
6. J. Fauveau, J.-P. Caltagirone, and M. Combarnous, Apparition d'écoulements thermoconvectifs multicellulaires dans une couche poreuse sphérique, *C. R. Acad. Sci. Ser. B*, vol. 287, pp. 285–288, 1978.
7. P. J. Burns, Convective Heat Transfer in Porous Insulation, Ph.D. thesis, Univ. of California, Berkeley, 1978.
8. J. Fauveau, Convection naturelle dans une couche poreuse limitée par deux surfaces sphériques concentriques, thesis no. 1477, Univ. of Bordeaux, 1979.